MEMS with fringing field: curvature-dependent electrostatic field and numerical techniques for recovering the membrane profile

[redacted]

[redacted]

MEMS with fringing field: curvature-dependent electrostatic field and numerical techniques for recovering the membrane profile

Mario Versaci[1] · **Paolo Di Barba**[2] · **Francesco Carlo Morabito**[1]

[redacted]

Abstract

As known, a $1D$ membrane MEMS semi-linear elliptic model with fringing field can be written as

$$u'' = -\frac{\lambda^2(1+\delta|u'|^2)}{(1-u)^2} \quad \text{in } \Omega \subset \mathbb{R}, \quad u = 0 \text{ on } \partial\Omega,$$

where λ^2 and δ are positive parameters and u is the deflection of the membrane. Since the electric field $\mathbf{E}$ on the membrane is locally orthogonal to the straight tangent line to the membrane, $|\mathbf{E}|$ can be considered locally proportional to the curvature K of the membrane, so that a well-known model with fringing field in which $|\mathbf{E}|^2 \propto \lambda^2/(1-u)^2$ has been here considered. In this paper, starting from this model, we present a new algebraic condition of uniqueness for the solution of this model depending on the electromechanical properties of the material constituting the membrane, which weighs more than the condition of existence known in literature. Furthermore, shooting-Dekker–Brent, Keller-Box-scheme, and III/IV Stage Lobatto IIIA formulas were exploited and their performances compared to recover u under convergence conditions in the presence/absence of ghost solutions. Finally, a criterion that is able to choose the material constituting the membrane starting from the applied electric voltage V and vice versa, in conditions of convergence, and in the presence and absence of ghost solutions, is presented.

Keywords MEMS devices · Fringing field · BVP semi-linear elliptic problems · Shooting and Keller-Box scheme · III/IV stage/Lobatto IIIA formulaes

Mathematics Subject Classification 30E25 · 35J65 · 35J93

[redacted]

✉ Mario Versaci
mario.versaci@unirc.it

[1] Dipartimento di Ingegneria Civile Energia Ambiente e Materiali, "Mediterranea" University, Via Graziella Feo di Vito, 89122 Reggio Calabria, Italy

[2] Dipartimento di Ingegneria Industriale e dell'Informazione, University of Pavia, Via A. Ferrata 5, Pavia, Italy

[redacted]

[redacted]

1 Introduction to the problem

Currently, industrial production addresses researchers and designers to develop low-cost devices combining the physical nature of problems and low-level machine languages. In this framework, both static and dynamic MEMS devices represent one of the most important achievements of engineering such that miniaturized/integrated electromechanical systems are required (Pelesko and Bernstein 2003; Ali 2012; Bechtold et al. 2013; Gad-el-Hak 2006; de Oliveira Hansen et al. 2018; Mohammadi and Ali 2015). Since the first MEMS was produced (Nathanson et al. 1964), scientific research has been involved in the development of models modeling the behavior of such devices under the most varied operating conditions. However, although these models are sophisticated, they often do not provide the solution explicitly, and thus, one has to be content with obtaining conditions ensuring existence and uniqueness of the solutions and avoiding any ghost solutions if the problem is solved numerically. In fact, numerical procedures could provide solutions which, if they do not respect the condition/conditions of existence and uniqueness, become ghost solutions (Angiulli et al. 2018; Versaci et al. 2019, 2020a, b; Versaci and Morabito 2019; Javaheri et al. 2018; Fento et al. 2018). MEMS can be employed from the design/construction of thermoelastic systems (Pelesko and Bernstein 2003; Howell and Luon 2004; Farokhi and Ghayesh 2017; Ren 2020) to biomedical applications (Pelesko and Bernstein 2003; Mistry and Mahapatra 2012; Di Barba et al. 2018, 2020; Di Barba and Wiak 2020). Theoretically, researchers hardly work in the manner testified by the conspicuous production of non-linear models obtaining useful conditions of existence and uniqueness of the solution (Cassani and Tarsia 2016; Cassani et al. 2009, 2013, 2014; Zozulya and Saez 2016; Cauchi 2018; Vinyas and Kattimani 2018). However, these sophisticated models provide conditions of existence and uniqueness independent of the material properties of the device, thereby having little response from the industry which requires simple models to implement. One of the most accredited models was studied in Cassani et al. (2009) that considered a dimensionless device comprising two parallel metal plates with a certain thickness. One was fixed and the other one deformable but anchored to the edges in which $u(x)$, $x \in \Omega$ with $\Omega = [-L, L] = [-0.5, 0.5]$ and $u(-L) = u(L) = 0$ is the profile of the deformable plate and the applied electrical voltage, V, pushes the deformable plate toward the fixed plate. However, since we need to consider membrane MEMS devices, we neglect the thickness of the deformable plate and the inertial effects. Therefore, in $1D$ dimensionless geometry, the model in Cassani et al. (2009) becomes the following:

$$\begin{cases} u''(x) = -\frac{\lambda^2}{(1-u(x))^2} & \text{in } \Omega \\ u(-L) = u(L) = 0. \end{cases} \tag{1}$$

where λ^2 is linked to V. In (1), the deformable plate is replaced by a membrane anchored at the edges to a metal plate. Then, if V is applied, the membrane deforms toward the upper plate, avoiding touching it (to avoid electrostatic discharges). Moreover, (1) concerns a membrane device without fringing field phenomenon (Leus and Elata 2004; Weng and Kong 1980; Chen et al. 2019; Gallalgher and Moussa 2014; Zhang 2018; Batra et al. 2006, 2007, 2006). However, if $d \not\ll L$, the fringing field must be considered (Oukad 2014, 2018; Mohammad and Oukad 2016). When only the outer solution for the electrostatic potential is used, the resulting elastic problem is (1) (Pelesko and Driscoll 2005). If the uniformly valid approximation for the electrostatic field $\mathbf{E}$ is used, the resulting elastic problem becomes (Pelesko and Driscoll 2005):

$$\begin{cases} u''(x) = -\frac{\lambda^2}{(1-u(x))^2} + \lambda^2 F(u(x), u'(x), \delta, \ldots) \ \text{ in } \Omega \\ u(-L) = u(L) = 0. \end{cases} \tag{2}$$

with F an appropriate function (see Pelesko and Driscoll 2005). Studying (1) means studying (2) neglecting $F(u(x), u'(x), \delta, \ldots)$ expecting that the effect of the neglected term is not significant. Moreover, $F(u(x), u'(x), \delta, \ldots)$ acts near the boundary, and most of the action in the deflection takes place far from the boundary. But is true for $\mathbf{E}$, while it is false for the electrostatic force. A close examination of the electrostatic force highlights that there are terms that arise when using the uniformly valid approximation to the $\mathbf{E}$ to evaluate the electrostatic force that act everywhere, not just at the boundary. Following this idea, we exploit the "corner-corrected theory" by Pelesko and Driscoll (2005) neglecting terms that only act in the boundary layer, including terms acting throughout the domain, obtaining the so-called corner-corrected model by examining each of the terms in (2) and ignoring those that are exponentially small away from the boundary. Therefore, (1) becomes (Pelesko and Driscoll 2005; Wei and Ye 2010)

$$\begin{cases} -u''(x) = \frac{\lambda^2(1+\delta|u'(x)|^2)}{(1-u(x))^2} \quad \text{in} \quad \Omega = [-L, L] \\ u(-L) = u(L) = 0. \end{cases} \tag{3}$$

which represent the corner corrected model where $\delta \geq 0$ and $\delta|u'(x)|^2$ concerns the fringing field phenomenon: if $\delta = 0$ (no fringing field), so that (3) becomes (1). Note that in (3) when $u'(x)$ becomes relevant the term $\delta|u'(x)|^2$ becomes significant. This occurs mostly at the boundary of the device. Hence the "corner-corrected theory" nomenclature. Electrostatically, the fringing field involves the bending of the electrostatic flow lines near the edge of the device with fringes of force lines (edge effect). Furthermore, the flow lines inside the device, far from the edges, are uniform and parallel. The same phenomenon can be observed in membrane MEMS devices: if the membrane deforms, an evident variation in the capacitance of the device is observed influenced by the variable distance between the membrane and the upper plate and accentuated by the fringing field. In (3), $\frac{\lambda^2}{(1-u(x))^2} \propto |\mathbf{E}|^2$. Thus:

$$u''(x) = -\theta|\mathbf{E}|^2, \quad \theta \in \mathbb{R}^+. \tag{4}$$

Moreover, as proved in Di Barba et al. (2017), $\mathbf{E}$ on the membrane is locally orthogonal to the straight line tangent to the membrane. Thus, $\mathbf{E} \propto K$, with K curvature of the membrane. As is known, K in $1D$ geometry is as follows:

$$K(x, u(x)) = |u''(x)|((1 + (u'(x))^2))^{-3/2}. \tag{5}$$

Thus, considering both (4) and (5), (3) becomes

$$\begin{cases} u''(x) = -\frac{1}{\theta\lambda^2}\frac{(1+(u'(x))^2)^3}{1+\delta|u'(x)|^2}(1 - u(x) - d^*)^2 \\ u(-L) = u(L) = 0, \quad 0 < u(x) < 1 - d^* \quad \text{in} \ \ (-L, L) \end{cases} \tag{6}$$

which represents a $1D$ second-order semi-linear elliptic model in which d^* (critical security distance) ensures that the membrane does not touch the upper plate. We observe that (6) does not yield explicit solutions so it is necessary to achieve conditions ensuring the existence/uniqueness of the solution. The work here presented is framed in a broader line of research which focuses the attention on membrane MEMS devices starting from the study of (1) where the singularity $1 - u(x)$ was present. The pioneering paper of this research is Di Barba et al. (2017) in which an elliptic semilinear model in 1D geometry was obtained starting from (1) where $\lambda^2/(1 - u(x))^2 \propto |\mathbf{E}|^2 \propto K^2(x, u(x))$ obtaining an elliptic semilinear

differential model in which the singularity is not explicitly evident. Since this model does not allow to obtain explicit solutions, the existence of the solution was studied by means of Schauder–Tychonoff fixed point techniques, obtaining an algebraic condition which, if satisfied, guaranteed the existence of the solution. Regarding uniqueness, in Di Barba et al. (2017) whatever the material constituting the membrane of the device was always guaranteed. In Angiulli et al. (2018) and Versaci et al. (2019), the uniqueness of the solution for model in Di Barba et al. (2017) was proved, however, finding an algebraic condition for the uniqueness dependent on the electromechanical properties of the material constituting the membrane which turned out to be stronger than the algebraic condition obtained in Di Barba et al. (2017) which governed existence. Therefore, the use of shooting techniques allowed to isolate any ghost solutions, also highlighting any fields of use of the device. Wondering if the model obtained in 1D geometry admitted possibly stable equilibrium configurations and if V must necessarily fall within a range of admissible values, in Di Barba et al. (2020) it was highlighted that the only equilibrium position obtained is characterized by instability and that the range of possible values for the external applicable voltage determines certain fields of applicability of the device. Furthermore, some energetic considerations have served as a prelude to the problem of optimal control. Subsequently, a lot of time was spent in generalizing in 2D geometry of what was elaborated in 1D (Di Barba et al. 2019). All this, both in 1D and 2D geometry, was processed without fringing field, so that the model was rewritten as in (3) to take into account the effect due to the fringing field both in 1D geometry (Di Barba et al. 2021) and in 2D geometry (paper in press) with attached study of the stability of the equilibrium positions, analysis of the range of possible values for the external voltage applied and study of the optimal control of the device.
The novelty of the present paper does not concern the suggestion of the model (6) but essentially concerns the following four points.

- To provide a new proof of the uniqueness of the solution for (6) depending on the electromechanical properties of the material constituting the membrane, highlighting that the condition obtained also depends on δ and, for $\delta = 0$, one obtains the same condition ensuring the uniqueness of the problem obtained in Di Barba et al. (2017) and Velosa-Moncada (2018).
- To obtain a single algebraic condition that ensures both the existence and the uniqueness of the solution depending on the electromechanical properties of the material constituting the membrane of the device, highlighting that, without fringing field, it can be superimposed with the algebraic condition obtained in Versaci et al. (2019).
- Shooting-Dekker–Brent procedure, Keller-Box scheme, and III/IV Stage Lobatto IIIa formulas, implemented in Matlab®R2017a running on an Intel Core 2 CPU at 1.45GHZ, have been exploited and compared to recover the membrane profile for different values of δ obtaining $\theta\lambda^2$ ensuring the convergence of the procedures. These techniques, well suited for non-linear BVPs, allow to detect the possible presence of the dreaded ghost solutions as the intensity of the effect due to the fringing field varies. Then, as $\theta\lambda^2$ changed under convergence conditions, the profiles of the membrane were reconstructed as δ increased within the range of its possible values. The results obtained showed a good symmetry of the recovered profiles even with intense fringing fields.
- Furthermore, ghost solutions were investigated obtaining $\inf\{V\}$ starting from which the membrane moves toward the upper plate. And again, the convergence areas with and without ghost solutions were obtained as the intensity of the fringing field varied. This study showed a good performance of the numerical approaches highlighting the areas of convergence in the presence of fairly contained ghost solutions. Finally, the ranges

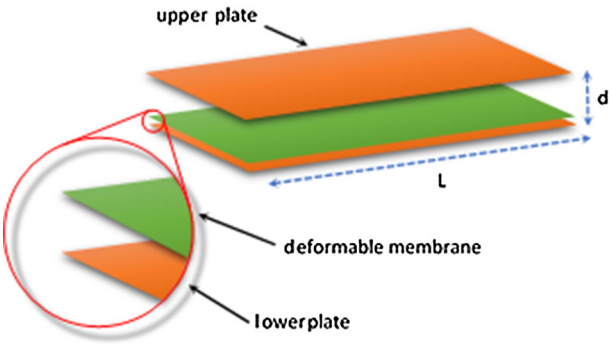

Fig. 1 Simplification of the device

of possible values of the electromechanical parameters of the material constituting the membrane were obtained both in the conditions of non-convergence/convergence with and without ghost solutions. This paper is organized as follows. A brief overview of the $1D$ electrostatic membrane MEMS device is presented in (Sect. 2), and the curvature-dependent $|\mathbf{E}|$ for modeling the membrane MEMS device with the fringing field is detailed in Sect. 3. Thereafter, Sect. 4 presents a well-known result of the existence of the solution for the problem under study, and Sect. 5 details the exploited procedure to achieve a new condition ensuring the uniqueness of the solution depending on the electromechanical properties of the membrane material . Therefore, a condition ensuring both the existence and uniqueness of the solution is achieved (see Sect. 6). Subsequently, Sect. 7 details the exploited numerical approaches, and Sect. 8 offers an in-depth overview of the numerical results obtained. Finally, some conclusions and future perspectives complete the work.

2 The 1D electrostatic membrane MEMS device

The device (Fig. 1) consists of two parallel metal plates placed at a distance d. We assume that the lower plate is located on the abscissa axis of a system of Cartesian axes Oxy and that when $V = 0$, the membrane remains in the resting position (i.e., the membrane rests on the lower plate so that $u(x) = 0\ \forall x \in [-L, L]$). If $V > 0$, the membrane deforms toward the upper plate so that $u(x) > 0$, $\forall x \in (-L, L)$, and $u(x) = 0$ if $x = \pm L$.
The geometry $1D$ of the device is such that $L \ll d$. Accordingly, the effect due to the fringing field is not negligible. Thus, (3) models the behavior of the device in which Pelesko and Bernstein (2003)

$$\lambda^2 = \frac{\epsilon_0 V^2 (2L)^2}{2d^3 T} = \rho V^2 \tag{7}$$

and

$$\rho = \frac{\epsilon_0 (2L)^2}{2d^3 T} \tag{8}$$

where ϵ_0 is the permittivity of the free space and T is the mechanical tension when the membrane is at rest. Considering that $\frac{\lambda^2}{(1-u(x))^2} \propto |\mathbf{E}|^2$, so that $\theta|\mathbf{E}|^2 = \frac{\lambda^2}{(1-u(x))^2}$, taking into account (7), we can write the following:

[redacted]

$$\theta|\mathbf{E}|^2 = \frac{\lambda^2}{(1-u(x))^2} = \frac{\epsilon_0 V^2 (2L)^2}{2d^3 T (1-u(x))^2}. \tag{9}$$

Remark 1 From (7), λ^2 is directly proportional to V^2, so λ^2 is bounded below by the fact that a minimum value of V is required to overcome the mechanical inertia of the membrane. On the other hand, V cannot increase indefinitely because its maximum value is fixed by the intended use of the device. Consequently, the value of λ^2 is also limited by the intended use of the device.

3 Curvature-dependent |E| for modeling membrane MEMS

As described above, $\mathbf{E}$ on the membrane is locally orthogonal to the straight line tangent to the membrane at the point considered. Electrostatically, this condition is because the outer membrane surface represents a physical interface between two media with different dielectric permittivity (membrane material and free space). Furthermore, the membrane imposes that $\mathbf{E}$ be orthogonal to the straight line tangent to the membrane at the point considered. Furthermore, we observe that if $\mathbf{E}$ is increased at one point on the membrane, it bends more at that point. Therefore, it is reasonable to express $|\mathbf{E}|$ depending on the curvature $K(x, u(x))$ of the membrane at the same point. So,

$$|\mathbf{E}| = \mu(x, u(x), \lambda) K(x, u(x)) \tag{10}$$

and, since when the membrane deforms it does not touch the upper plate (to avoid electrostatic discharges), a possible formulation for $\mu(x, u(x), \lambda)$ can be $\mu(x, u(x), \lambda) = \frac{\lambda}{1-u(x)-d^*}$, where $\mu(x, u(x), \lambda) \in C^0([-L, L] \times [0, 1) \times [0, \lambda_{max}]$. Therefore, model (3), taking account both (4) and (10), becomes

$$\begin{cases} u''(x) = -\frac{\lambda^2(1+\delta|u'(x)|^2)}{(1-u(x))^2} = \theta|\mathbf{E}|^2(1+\delta|u'(x)|^2) = -\theta\frac{\lambda^2(1+\delta|u'(x)|^2)}{(1-u(x)-d^*)^2} K^2(x, u(x)) \\ u(-L) = u(L) = 0, \quad 0 < u(x) < 1 - d^* \quad \text{in } (-L, L), \quad \theta \in \mathbb{R}^+, \end{cases} \tag{11}$$

and considered that, in $1D$ geometry, $K(x, u(x))$ is expressible as (5), (3) becomes

$$\begin{cases} u''(x) = -\theta\frac{\lambda^2(1+\delta|u'(x)|^2)}{(1-u(x)-d^*)^2}\frac{|u''(x)|^2}{(1+(u'(x))^2)^3} \\ u(-L) = u(L) = 0, \quad 0 < u(x) < 1 - d^* \quad \text{in } (-L, L), \quad \theta \in \mathbb{R}^+ \end{cases} \tag{12}$$

from which

$$\begin{cases} u''(x) = -\frac{1}{\theta\lambda^2}\frac{(1+(u'(x))^2)^3}{(1+\delta|u'(x)|^2)}(1-u(x)-d^*)^2 \\ u(-L) = u(L) = 0, \quad 0 < u(x) < 1 - d^* \quad \text{in } (-L, L), \quad \theta \in \mathbb{R}^+. \end{cases} \tag{13}$$

Remark 2 To obtain (13) from (12), we assume $u''(x) \neq 0$. This is true because if $u''(x) = 0$, it would follow $u'(x) = k$ (k arbitrary constant), and $u(x) = kx + b$ (b arbitrary constant). In other words, we would obtain a linear deflection when $|\mathbf{E}| = 0$. This is an evidently impossible condition. Thus, $u''(x) \neq 0$. Moreover, being $\delta \geq 0$ and $|u'(x)| \geq 0$, it follows that $1 + \delta|u'(x)|^2 \neq 0$ so that (13) makes sense. Finally, being $\theta \in \mathbb{R}^+$ and $\lambda^2 \geq 0$, $\theta\lambda^2 > 0$ and $\frac{1}{\theta\lambda^2} > 0$ so that (13) makes sense. Particularly, $\theta \in \mathbb{R}^+$ ensures that the membrane deforms toward the upper plate. This is because from $-u''(x) = \theta|\mathbf{E}|^2$ being $\theta > 0$, the membrane is concave and on applying an external $V > 0$ (i.e., by (7), $\lambda^2 > 0$), the membrane moves toward the upper plate instead of adhering to the lower plane.

Remark 3 (13), apparently, does not present the singularity $\frac{1}{(1-u(x))^2}$ evident in (3). However, if in (13) $u(x)$ is equal to $1-d^*$ (i.e., equal to the value generating singularity in (13)) $u''(x)$ would be 0, and considering (4), it would follow that $|\mathbf{E}| = 0$ producing, as observed in Remark 2, a linear deflection of the membrane (unacceptable occurrence).

Remark 4 Analitically, θ has no limitations except that it must obviously both be non-zero. However, we will see later that $\theta\lambda^2$ will suffer specific limitations due to problems of convergence of the numerical procedures in the presence/absence of ghost solutions.

Remark 5 Concerning $\mu(x, u(x), \lambda)$ proportionality function, there are no obvious limitations to the values attribuable to it.

Remark 6 (13) is a particular case of the following general problem (Bayley et al. 1969; Di Barba et al. 2019; Zega et al. 2018):

$$\begin{cases} u''(x) = -f(x, u(x), u'(x)) \\ u(-L) = u(L) = 0, \quad 0 < u(x) < 1 - d^* \quad \text{in } (-L, L) \end{cases} \tag{14}$$

where $f \in C^0([-L, L] \times \mathbb{R} \times \mathbb{R})$. Obviously, in our case, we have

$$f(x, u(x), u'(x)) = \frac{1}{\theta\lambda^2} \frac{(1 + (u'(x))^2)^3}{(1 + \delta|u'(x)|^2))} (1 - u(x) - d^*)^2 \tag{15}$$

and $u(x) \in C^2([-L, L])$, ensuring that the membrane does not have tears, and moreover, its slope varies continuously. The need to write the problem under study in general terms arises from the fact that this generalization allows to use general results of existence and uniqueness of the solution as consolidated in the literature, relating to the class of BVPs.

Remark 7 If the membrane is too thin, wrinkling is highly likely. However, to formulate $K(x, u(x))$ it is necessary that $u(x) \in C^2([-L, L])$ implying that abrupt local variations of the membrane profile are not allowed.

Remark 8 (13) needs to be studied on dependence on the range of δ in which the device is operated and the actual material's dependence of electrical conductivity on, for example, the temperature. This phenomenon help us to understand if the system changes behavior as δ varied (bifurcation). However, in this paper, we will limit ourselves to obtaining a limitation for δ due to a solution existence result for (13), postponing more solid results regarding the bifurcation study to future work.

4 An interesting result of existence

In the following, we need to introduce a functional space.

Definition 1 Let us consider the functional space P defined as follows:

$$P = \{C_0^2([-L, L]) : \ 0 < u(x) < 1 - d^*, \ \ |u'(x)| < H\}. \tag{16}$$

The existence of the solution, and particularly the following proposition, has been proved in Di Barba et al. (2021) exploiting the Schauder–Tychonoff fixed point theorem.

[redacted]

Proposition 1 (13) *admits at least one solution. Moreover, the following inequality holds:*

$$H < \sqrt[6]{\frac{\theta\lambda^2}{2L^2(2-\delta)\alpha}}, \tag{17}$$

and it ensures the existence of at least one solution for (13)*. Moreover, numerically, the following was achieved* $H = 146$ *(for some details, see below).*

Remark 9 From (17) and without fringing field (i.e., $\delta = 0$), one gets

$$H < \sqrt[6]{\frac{\theta\lambda^2}{2L^2\alpha}} \tag{18}$$

which makes sense because $L^2\alpha > 0$ and $\theta\lambda^2 > 0$. Moreover, with the fringing field, it is imperative that $\frac{\theta\lambda^2}{2L^2(2-\delta)\alpha} \geq 0$. In other words, since $\theta\lambda^2 > 0$, $2 - \delta > 0$, and finally $\delta < 2$. Therefore,

$$0 < \delta < 2. \tag{19}$$

Thus, for the device under study, δ cannot grow indefinitely (as mathematically hypothesized in the literature) but is limited by (19).

5 A condition ensuring the uniqueness of the solution

As introduced in the previous section, we present here an algebraic condition ensuring the uniqueness of the solution for (13) depending on the electromechanical properties of the material constituting the membrane.

Proposition 2 *The algebraic condition ensuring the uniqueness of the solution for* (13) *is as follows:*

$$1 + H^6 < \frac{\theta\lambda^2}{24L(L+1)(1-\delta H^2)}. \tag{20}$$

Proof We observe that (14), by a suitable Green's function $G(x, s)$, can be rewritten in its equivalent integral formulation (Bayley et al. 1969)

$$u(x) = \int_{-L}^{L} G(x, s) f(x, u(x), u'(x))\mathrm{d}s \tag{21}$$

and considering (15), (21) becomes :

$$u(x) = \int_{-L}^{L} G(x, s) \frac{1}{\theta\lambda^2} \frac{(1 + (u_1'(x))^2)^3}{(1 + \delta|u_1'(x)|^2))} (1 - u_1(x) - d^*)^2 \mathrm{d}s, \tag{22}$$

where (Bayley et al. 1969)

$$G(x, s) = \frac{(s + L)(L - x)}{2L} \tag{23}$$

if $-L \leq s \leq x$ and

$$G(x, s) = \frac{(L - s)(x + L)}{2L} \tag{24}$$

[redacted]

when $x \leq s \leq L$. Moreover,

$$G_x(x,s) = -\frac{(s+L)}{2L} \tag{25}$$

if $-L \leq s < x$ and

$$G_x(x,s) = \frac{(L-s)}{2L} \tag{26}$$

when $x < s \leq L$. Moreover, it is easy to prove that (Bayley et al. 1969)

$$0 \leq G(x,s) \leq \frac{L}{2} \quad \forall x, s \in [-L, L], \tag{27}$$

$$\int_{-L}^{L} G(x,s)\mathrm{d}s = \frac{(L-x)(x+L)}{2} \leq \frac{L^2}{2} \tag{28}$$

and

$$\left| \int_{-L}^{L} G_x(x,s)\mathrm{d}s \right| \leq \int_{-L}^{L} |G_x(x,s)|\mathrm{d}s < L, \tag{29}$$

$$\forall (x,s) \in ([-L,L] \times [-L,L]), \quad G_x(x,s) \leq \frac{1}{2}. \tag{30}$$

By contradiction, we assume that u_1 and u_2, both belonging to P, are two different solutions for (13), so that $u_1 = T(u_1)$ and $u_2 = T(u_2)$. Therefore,

$$u_i(x) = T(u_1(x)) = \int_{-L}^{L} G(x,s)\frac{1}{\theta\lambda^2}\frac{(1+(u_i'(x))^2)^3}{(1+\delta|u_i'(x)|^2))}(1-u_i(x)-d^*)^2\mathrm{d}s \tag{31}$$

for $i = 1, 2$ from which

$$u_i'(x) = T'(u_1(x)) = \int_{-L}^{L} G_x(x,s)\frac{1}{\theta\lambda^2}\frac{(1+(u_i'(x))^2)^3}{(1+\delta|u_i'(x)|^2))}(1-u_i(x)-d^*)^2\mathrm{d}s \tag{32}$$

Therefore, we can write the following:

$$\begin{aligned}
&\|u_1(x) - u_2(x)\|_{C^1([-L,L])} \\
&= \sup_{x\in[-L,L]} |u_1(x) - u_2(x)| + \sup_{x\in[-L,L]} |u_1'(x) - u_2'(x)| \\
&= \sup_{x\in[-L,L]} \left| \int_{-L}^{L} \frac{G(x,s)}{\theta\lambda^2}\frac{(1+(u_1'(x))^2)^3}{(1+\delta|u_1'(x)|^2))}(1-u_1(x)-d^*)^2\mathrm{d}s \right. \\
&\quad \left. - \int_{-L}^{L} \frac{G(x,s)}{\theta\lambda^2}\frac{(1+(u_2'(x))^2)^3}{(1+\delta|u_2'(x)|^2))}(1-u_2(x)-d^*)^2\mathrm{d}s \right| \\
&\quad + \sup_{x\in[-L,L]} \left| \int_{-L}^{L} \frac{G_x(x,s)}{\theta\lambda^2}\frac{(1+(u_1'(x))^2)^3}{(1+\delta|u_1'(x)|^2))}(1-u_1(x)-d^*)^2\mathrm{d}s \right. \\
&\quad \left. - \int_{-L}^{L} \frac{G_x(x,s)}{\theta\lambda^2}\frac{(1+(u_2'(x))^2)^3}{(1+\delta|u_2'(x)|^2))}(1-u_2(x)-d^*)^2\mathrm{d}s \right| \\
&= \frac{1}{\theta\lambda^2} \sup_{x\in[-L,L]} \left| \int_{-L}^{L} G(x,s)\frac{(1+(u_1'(x))^2)^3}{(1+\delta|u_1'(x)|^2))}(1-u_1(x)-d^*)^2\mathrm{d}s \right. \\
&\quad \left. - \int_{-L}^{L} G(x,s)\frac{(1+(u_2'(x))^2)^3}{(1+\delta|u_2'(x)|^2))}(1-u_2(x)-d^*)^2\mathrm{d}s \right|
\end{aligned}$$

[redacted]

$$
\begin{aligned}
&+\frac{1}{\theta\lambda^2}\sup_{x\in[-L,L]}\left|\int_{-L}^{L}G_x(x,s)\frac{(1+(u_1'(x))^2)^3}{(1+\delta|u_1'(x)|^2))}(1-u_1(x)-d^*)^2\mathrm{d}s\right.\\
&\left.-\int_{-L}^{L}G_x(x,s)\frac{(1+(u_2'(x))^2)^3}{(1+\delta|u_2'(x)|^2))}(1-u_2(x)-d^*)^2\mathrm{d}s\right|\\
&=\frac{1}{\theta\lambda^2}\sup_{x\in[-L,L]}\left|\int_{-L}^{L}G(x,s)\left\{\frac{(1+(u_1'(x))^2)^3}{(1+\delta|u_1'(x)|^2))}(1-u_1(x)-d^*)^2\right.\right.\\
&\left.\left.-\frac{(1+(u_2'(x))^2)^3}{(1+\delta|u_2'(x)|^2))}(1-u_2(x)-d^*)^2\right\}\mathrm{d}s\right|\\
&+\frac{1}{\theta\lambda^2}\sup_{x\in[-L,L]}\left|\int_{-L}^{L}G_x(x,s)\left\{\frac{(1+(u_1'(x))^2)^3}{(1+\delta|u_1'(x)|^2))}(1-u_1(x)-d^*)^2\right.\right.\\
&\left.\left.-\frac{(1+(u_2'(x))^2)^3}{(1+\delta|u_2'(x)|^2))}(1-u_2(x)-d^*)^2\right\}\mathrm{d}s\right|\\
&\le\frac{1}{\theta\lambda^2}\sup_{x\in[-L,L]}\int_{-L}^{L}|G(x,s)|\left|\frac{(1+(u_1'(x))^2)^3}{(1+\delta|u_1'(x)|^2))}(1-u_1(x)-d^*)^2\right.\\
&\left.-\frac{(1+(u_2'(x))^2)^3}{(1+\delta|u_2'(x)|^2))}(1-u_2(x)-d^*)^2\right|\mathrm{d}s\\
&+\frac{1}{\theta\lambda^2}\sup_{x\in[-L,L]}\int_{-L}^{L}|G_x(x,s)|\left|\frac{(1+(u_1'(x))^2)^3}{(1+\delta|u_1'(x)|^2))}(1-u_1(x)-d^*)^2\right.\\
&\left.-\frac{(1+(u_2'(x))^2)^3}{(1+\delta|u_2'(x)|^2))}(1-u_2(x)-d^*)^2\right|\mathrm{d}s.
\end{aligned}
\tag{33}
$$

Considering both (27) and (29), (33) becomes the following:

$$
\begin{aligned}
&\|u_1(x)-u_2(x)\|_{C^1([-L,L])}\\
&\le\frac{L}{2\theta\lambda^2}\sup_{x\in[-L,L]}\int_{-L}^{L}\left|\frac{(1+(u_1'(x))^2)^3}{(1+\delta|u_1'(x)|^2))}(1-u_1(x)-d^*)^2\right.\\
&\left.-\frac{(1+(u_2'(x))^2)^3}{(1+\delta|u_2'(x)|^2))}(1-u_2(x)-d^*)^2\right|\mathrm{d}s\\
&+\frac{1}{2\theta\lambda^2}\sup_{x\in[-L,L]}\int_{-L}^{L}\left|\frac{(1+(u_1'(x))^2)^3}{(1+\delta|u_1'(x)|^2))}(1-u_1(x)-d^*)^2\right.\\
&\left.-\frac{(1+(u_2'(x))^2)^3}{(1+\delta|u_2'(x)|^2))}(1-u_2(x)-d^*)^2\right|\mathrm{d}s\\
&=\left(\frac{L}{2\theta\lambda^2}+\frac{1}{2\theta\lambda^2}\right)\sup_{x\in[-L,L]}\int_{-L}^{L}\left|\frac{(1+(u_1'(x))^2)^3}{(1+\delta|u_1'(x)|^2))}(1-u_1(x)-d^*)^2\right.\\
&\left.-\frac{(1+(u_2'(x))^2)^3}{(1+\delta|u_2'(x)|^2))}(1-u_2(x)-d^*)^2\right|\mathrm{d}s.
\end{aligned}
\tag{34}
$$

To achieve (20), we need to exploit the following result (see (35)) proved in Versaci et al. (2019). Particularly, considering that $\alpha=1-d^*<1$, $\forall u_1(x),u_2(x)\in P$, the following inequality holds (Versaci et al. 2019):

[redacted]

$$|(1+(u_2'(x))^2)^3(1-u(x)-d^*)^2-(1+(u_1'(x))^2)^3(1-u(x)-d^*)^2|$$
$$\le 216H^5|u_2'(x)-u_1'(x)|+24(1+H^6)|u_2(x)-u_1(x)|. \tag{35}$$

However, considering

$$\frac{1}{1+\delta(u'(x))^2}=\frac{1+\delta(u'(x))^2-\delta(u'(x))^2}{1+\delta(u'(x))^2}$$
$$\le 1+\delta(u'(x))^2-\delta(u'(x))^2\le 1+\delta H^2-\delta(u'(x))^2\le 1+\delta H^2, \tag{36}$$

we can write the following:

$$\left|\frac{(1+(u_1'(x))^2)^3}{(1+\delta|u_1'(x)|^2))}(1-u_1(x)-d^*)^2\right.$$
$$\left.-\frac{(1+(u_2'(x))^2)^3}{(1+\delta|u_2'(x)|^2))}(1-u_2(x)-d^*)^2\right|$$
$$\le\frac{(1+(u_1'(x))^2)^3}{(1+\delta|u_1'(x)|^2))}(1-u_1(x)-d^*)^2$$
$$+\frac{(1+(u_2'(x))^2)^3}{(1+\delta|u_2'(x)|^2))}(1-u_2(x)-d^*)^2$$
$$\le\Big[(1+(u_1'(x))^2)^3(1-u_1(x)-d^*)^2$$
$$+(1+(u_2'(x))^2)^3(1-u_2(x)-d^*)^2\Big](1+\delta H^2). \tag{37}$$

But

$$|(1+(u_2'(x))^2)^3(1-u(x)-d^*)^2-(1+(u_1'(x))^2)^3(1-u(x)-d^*)^2|$$
$$\le(1+(u_1'(x))^2)^3(1-u_1(x)-d^*)^2+(1+(u_2'(x))^2)^3(1-u_2(x)-d^*)^2, \tag{38}$$

which becomes

$$|(1+(u_2'(x))^2)^3(1-u(x)-d^*)^2$$
$$-(1+(u_1'(x))^2)^3(1-u(x)-d^*)^2|(1+\delta H^2)$$
$$\le\Big[(1+(u_1'(x))^2)^3(1-u_1(x)-d^*)^2$$
$$+(1+(u_2'(x))^2)^3(1-u_2(x)-d^*)^2\Big](1+\delta H^2). \tag{39}$$

Therefore, taking into account (35), (37) becomes:

$$\left|\frac{(1+(u_1'(x))^2)^3}{(1+\delta|u_1'(x)|^2))}(1-u_1(x)-d^*)^2\right.$$
$$\left.-\frac{(1+(u_2'(x))^2)^3}{(1+\delta|u_2'(x)|^2))}(1-u_2(x)-d^*)^2\right|$$
$$\le\{216H^5|u_2'(x)-u_1'(x)|$$
$$+24(1+H^6)|u_2(x)-u_1(x)|\}(1-\delta H^2). \tag{40}$$

[redacted]

Thus, $\|u_2(x)-u_1(x)\|_{C^1([-L,L])}$, considering both (34) and (40) and exploiting the theorem of the mean of integrals, the result is as follows:

$$
\begin{aligned}
&\|u_2(x)-u_1(x)\|_{C^1([-L,L])}\\
&\le \Big(\frac{L}{2\theta\lambda^2}+\frac{1}{2\theta\lambda^2}\Big)\sup_{x\in[-L,L]}\int_{-L}^{L}\left|\frac{(1+(u_1'(s))^2)^3}{(1+\delta|u_1'(s)|^2))}(1-u_1(s)-d^*)^2\right.\\
&\quad\left.-\frac{(1+(u_2'(s))^2)^3}{(1+\delta|u_2'(s)|^2))}(1-u_2(s)-d^*)^2\right|\mathrm{d}s\\
&\le \Big(\frac{L}{2\theta\lambda^2}+\frac{1}{2\theta\lambda^2}\Big)\sup_{x\in[-L,L]}\int_{-L}^{L}\{216H^5|u_2'(s)-u_1'(s)|\\
&\quad+24(1+H^6)|u_2(s)-u_1(s)|\}(1-\delta H^2)\mathrm{d}s\\
&\le \Big(\frac{L}{2\theta\lambda^2}+\frac{1}{2\theta\lambda^2}\Big)\sup_{x\in[-L,L]}\left\{\int_{-L}^{L}216H^5|u_2'(s)-u_1'(s)|(1-\delta H^2)\mathrm{d}s\right.\\
&\quad\left.+\int_{-L}^{L}24(1+H^6)|u_2(s)-u_1(s)|\}(1-\delta H^2)\mathrm{d}s\right\}\\
&= \Big(\frac{L}{2\theta\lambda^2}+\frac{1}{2\theta\lambda^2}\Big)\sup_{x\in[-L,L]}\left\{216H^5(1-\delta H^2)\int_{-L}^{L}|u_2'(s)-u_1'(s)|\mathrm{d}s\right.\\
&\quad\left.+24(1+H^6)(1-\delta H^2)\int_{-L}^{L}|u_2(s)-u_1(s)|\}\mathrm{d}s\right\}\\
&= \Big(\frac{L}{2\theta\lambda^2}+\frac{1}{2\theta\lambda^2}\Big)\left\{216H^5(1-\delta H^2)\sup_{x\in[-L,L]}\int_{-L}^{L}|u_2'(s)-u_1'(s)|\mathrm{d}s\right.\\
&\quad\left.+24(1+H^6)(1-\delta H^2)\sup_{x\in[-L,L]}\int_{-L}^{L}|u_2(s)-u_1(s)|\}\mathrm{d}s\right\}\\
&= \Big(\frac{L}{2\theta\lambda^2}+\frac{1}{2\theta\lambda^2}\Big)216H^5(1-\delta H^2)2L\sup_{x\in[-L,L]}|u_2'(x)-u_1'(x)|\\
&\quad+\Big(\frac{L}{2\theta\lambda^2}+\frac{1}{2\theta\lambda^2}\Big)24(1+H^6)2L(1-\delta H^2)\sup_{x\in[-L,L]}|u_2(x)-u_1(x)|. \qquad (41)
\end{aligned}
$$

From (41), to obtain a contradiction, it is necessary that

$$
\begin{cases}
2L\Big(\frac{L}{2\theta\lambda^2}+\frac{1}{2\theta\lambda^2}\Big)216H^5(1-\delta H^2)<1\\
2L\Big(\frac{L}{2\theta\lambda^2}+\frac{1}{2\theta\lambda^2}\Big)24(1+H^6)(1-\delta H^2)<1
\end{cases} \qquad (42)
$$

from which

$$
\begin{cases}
1+H^6<1+\frac{H\theta\lambda^2}{216L(L+1)(1-\delta H^2)}\\
1+H^6<1+\frac{\theta\lambda^2}{24L(L+1)(1-\delta H^2)}.
\end{cases} \qquad (43)
$$

In (43), we note that

$$
1+\frac{\theta\lambda^2}{24L(L+1)(1-\delta H^2)}<1+\frac{H\theta\lambda^2}{216L(L+1)(1-\delta H^2)}. \qquad (44)
$$

In fact, if absurdly

$$1+\frac{\theta\lambda^2}{24L(L+1)(1-\delta H^2)} > 1+\frac{H\theta\lambda^2}{216L(L+1)(1-\delta H^2)}, \tag{45}$$

we would obtain $1 > \frac{H}{9} = \frac{146}{9} = 16.22$ which is a condition that is clearly false. Therefore, (20) holds.

6 A condition ensuring both existence and uniqueness

Proposition 3 *The algebraic condition* (20) *ensures the existence and uniqueness of the solution for problem* (13).

Proof As both (17) and (20) are verified, we can write the following:

$$\begin{cases} H^6 < \frac{\theta\lambda^2}{2L^2(2-\delta)\alpha} & \text{(existence)} \\ H^6 < \frac{\theta\lambda^2}{24L(L+1)(1-\delta H^2)} - 1 & \text{(uniqueness).} \end{cases} \tag{46}$$

It is easy to prove that system (46) is equivalent to (20). In fact

$$\frac{\theta\lambda^2}{24L(L+1)(1-\delta H^2)} - 1 < \frac{\theta\lambda^2}{2L^2(2-\delta)\alpha}. \tag{47}$$

This is since $2-\delta > 0$, $\frac{\theta\lambda^2}{2L^2(2-\delta)\alpha}$ is always positive, while $\frac{\theta\lambda^2}{24L(L+1)(1-\delta H^2)} - 1$, making $1-\delta H^2 < 0$ negative. Therefore, the condition ensuring both the existence and uniqueness of the solution for (13) is (20). □

Remark 10 Unlike (Versaci et al. 2020b), the algebraic condition of existence and uniqueness for the solution (see (20)) with fringing field does not depend on d^* that can be chosen as small as you like. This is important for the search for possible equilibrium positions of the membrane profile and relative stability. Obviously, if $\delta = 0$, we obtain the same condition known in Di Barba et al. (2017) and Velosa-Moncada (2018) without fringing field. Finally, (20), given the presence of $\theta\lambda^2$, depends on the electromechanical properties of the material constituting the membrane.

7 The exploited numerical approaches

7.1 Shooting and Dekker–Brent procedure

We transform (13) into an equivalent system of first order differential equations considering (Quarteroni et al. 2007):

$$u_1(x) = u(x), \quad u_2(x) = u'(x) \tag{48}$$

so that from (13) we obtain the following:

$$\begin{cases} u_1'(x) = f(u_1(x), u_2(x)) = u_2(x) \\ u_2'(x) = g(u_1(x), u_2(x)) = -\frac{1}{\theta\lambda^2}\frac{(1+(u_2'(x))^2)^3}{1+\delta(u_2(x))^2}(1-u_1(x)-d^*)^2. \end{cases} \tag{49}$$

[redacted]

(49) is transformed into an equivalent IVP by replacing the boundary condition of the solution $u_1(L)$ at $x = L$ with $u_2(-L) = \eta$, $\eta \in \mathbb{R}^+$ as an initial condition. Thus, the non-linear equation $F(\eta) = u_1(L; \eta) = 0$ is defined iteratively solvable to achieve η.

7.1.1 Zeros of $F(\eta)$: the Dekker–Brent approach

To solve $F(\eta) = 0$, we exploit the Dekker–Brent approach. At each iteration, three points are involved: b_k which approximates the zero temporarily; a_k, the "contra-point", such that $F(a_k)$ and $F(b_k)$ have opposite signs, and the interval $[a_0, b_0]$ contains the solution; b_{k-1} which represents the value of b from the previous iteration. Thus, two temporary values are computed: the first is obtained through a procedure based on the secant method; the second is obtained through a bisection procedure. Particularly,

$$\begin{cases} s = b_k - \frac{b_k - b_{k-1}}{F(b_k) - F(b_{k-1})} F(b_k), & \text{if} \quad F(b_k) \neq F(b_{k-1}), \\ s = m = \frac{a_k + b_k}{2}, & \text{otherwise.} \end{cases} \tag{50}$$

Since s is included between b_k and m, $s = b_{k+1}$, otherwise $m = b_{k+1}$. Then, the new contra-point will be selected so that $F(a_{k+1})$ and $F(b_{k+1})$ have different signs. In this case, $a_{k+1} = a_k$, otherwise $a_{k+1} = b_k$. Finally, if $|F(a_{k+1})| \leq |F(b_{k+1})|$, a_{k+1} is the best approximation of the solution with respect to b_{k+1}, and a_{k+1} and b_{k+1} are interchangeable. However, if the procedure is based on the secant method, b_k converges slowly. To avoid this issue, Brent's procedure considers a test to be satisfied before the result obtained can be accepted at the next iteration. Considering δ_1 as a tolerance, if in the previous step the secant method was used,

$$|\delta_1| < |b_k - b_{k-1}| \tag{51}$$

and

$$|\delta_1| < |s - b_k| < \frac{1}{2}|b_k - b_{k-1}|, \tag{52}$$

and this must be applied to decide whether to perform interpolation or bisection. The Brent modification ensures that at the k^{th} iteration, the bisection-based procedure is used at least a number of times equal to $2\log_2(|b_{k-1} - b_{k-2}|/\delta_1)$. Furthermore, the Brent approach uses a numerically more efficient inverse quadratic interpolations instead of linear interpolations. If $F(b_k)$, $F(a_k)$ and $F(b_{k-1})$ are different, the efficiency of the method increases slightly. Therefore, the condition for accepting s must be changed: s must be contained in $[\frac{3a_k + b_k}{4}, b_k]$. To obtain the solution of $F(\eta) = 0$, we obtain a η_k related to the IVP. Then, a stop text is used to verify that $\eta_k \to \eta$ as $k \to +\infty$. In this work, two MatLab® routines *ode*23 and *ode*45 were used to integrate the IVPs, using the accuracy defined by default. Finally, instability phenomena could take place to yield the solution of the IVPs. This affects the solutions of the respective BVPs which could be insensitive to the variations of the boundary values. Shooting techniques have also been used successfully in the recent past from other Authors in the MEMS domain as evidenced, for example, in Zhao (2004) and Yu (2012). We note that the MEMS membrane device here studied is not in the regime of large displacement. In fact, as revealed by numerical simulations here performed (see figures below), the recovering of the membrane profiles highlighted small displacements putting in evidence that the device can be appropriate, for example, in biomedical application as intravenous drug diffuse system, where small movements of the membrane are required.

7.2 Relaxation and Keller Box scheme

It is necessary to make a mesh of points, $x_0 = -L_1$, $x_j = x_0 + j\Delta x$, for $j = 1, 2, \ldots, J$, spaced with $x_J = L_1$. By $\mathbf{u}_j$, $j = 0, 1, \ldots, J$, we denote the numerical approximation to the solution $\mathbf{u}(x_j)$ of (49). Thus, the Keller-Box scheme is writable as (Quarteroni et al. 2007)

$$\begin{cases} \mathbf{u}_j - \mathbf{u}_{j-1} - \Delta\mathbf{F}\left(x_{j-1/2}\frac{\mathbf{u}_j+\mathbf{u}_{j-1}}{2}\right) = \mathbf{0}, & j = 1, \cdots, J \\ \mathbf{G}(\mathbf{u}_0, \mathbf{u}_J) = \mathbf{0}, & x_{j-1/2} = (x_j + x_{j-1})/2 \end{cases} \tag{53}$$

which represents a system of non-linear equations with $2(J + 1)$ unknowns. Furthermore, a termination criterion, such as

$$\frac{1}{2(J+1)} \sum_{\ell=1}^{2} \sum_{j=0}^{J} |\Delta u_{j\ell}| \leq \text{TOL} \tag{54}$$

must be applied in which $\Delta u_{j\ell}$, $j = 0, 1, \ldots, J$ and $\ell = 1, 2$ is the difference between two successive iterate components and TOL is a fixed tolerance. The simulations produced with this numerical procedure also showed recovering of the membrane profile in conditions of small displacements, highlighting fields of applicability in the biomedical field of the device. Unlike the shooting method, Keller-Box scheme in MEMS is scarcely used for the resolution of BVPs because it requires higher computational efforts requiring more complex hardware for any industrial applications. However, in this paper, we considered it appropriate to use this methodology as well to make a more effective comparison between numerical procedures.

7.3 Collocation procedure and III/IV stage Lobatto IIIa formulas

7.3.1 Collocation approach

(49) can be written as follows Quarteroni et al. (2007):

$$\frac{\mathrm{d}\mathbf{u}(r)}{\mathrm{d}r} = \mathbf{F}(r, \mathbf{u}(r)) \tag{55}$$

with suitable boundary conditions. Thus, from (55),

$$\mathbf{u}(x) = \mathbf{u}(x_n) + \int_{x_n}^{x} \mathbf{F}(r, \mathbf{u}(r))\mathrm{d}r, \tag{56}$$

and, replacing $\mathbf{u}(x_n)$ by $\mathbf{u}_n$ (approximated value), we have the following:

$$\mathbf{u}(x) \approx \mathbf{u}_n + \int_{x_n}^{x} \mathbf{p}(r)\mathrm{d}r, \tag{57}$$

where $\mathbf{p}(r)$ is an interpolation polynomial whose degree is lower than s, interpoling $[x_{n,i}, \mathbf{F}(x_{n,i}), \mathbf{u}(x_{n,i})]$, $i = 1, 2, \ldots, s$, and $x_{n,i} = x_n + \tau_i h, \quad i = 1, \ldots, s$, $0 \leq \tau_1 < \cdots < \tau_s \leq 1$.. Moreover, exploiting the Lagrange fundamental polynomials $\mathbf{L}_j(r)$, $\mathbf{p}(r) = \sum_{j=1}^{s} \mathbf{F}(x_{n,j}, \mathbf{u}(x_{n,j}))\mathbf{L}_j(r)$, so that

$$\mathbf{u}(x) \approx \mathbf{u}_n + \sum_{j=1}^{s} \mathbf{F}(x_{n,j}, \mathbf{u}(x_{n,j})) \int_{x_n}^{x} \mathbf{L}_j(r)\mathrm{d}r. \tag{58}$$

[redacted]

Therefore, (58) is forced $\forall x_{n,j}$, so that $\mathbf{u}_{n,j}$ at collocation node points are carried out, for $i = 1, \ldots, s$, by:

$$\mathbf{u}_{n,j} = \mathbf{u}_n + \sum_{j=1}^{s} \mathbf{F}(x_{x_{n,i}}, \mathbf{u}_{n_{n,j}}) \int_{x_n}^{x_{n,i}} \mathbf{L}_j(r)\mathrm{d}r. \tag{59}$$

Remark 11 (59) can be implemented by several programming languages, so that it can be exploited for several membrane MEMS device applications in which the production of the microchips is low cost.

7.3.2 The implicit Runge–Kutta methods (RK)

$\mathbf{F}(x, \mathbf{u}(x))$ must be evaluated several times in each $[x_n, x_{n+1}]$. Moreover, $u_{n+1} = u_n + h\sum_{i=1}^{s} b_i k_i$ where $k_i = \mathbf{F}\Big(x_n + c_i h, u_n + h\sum_{j=1}^{s} a_{ij}k_j\Big)$, $i = 1, 2, \ldots, s$, with s is the number of stage (Quarteroni et al. 2007). Usually, to make an implicit RK procedure, it is necessary to consider the following three conditions:

$$B(p) : \sum_{i=1}^{s} b_i c_i^{k-1} = k^{-1}, \quad k = 1, 2, \ldots, p, \tag{60}$$

$$C(q) : \sum_{i=1}^{s} a_{ij} c_i^{k-1} = k^{-1} c_i^k, \quad k = 1, 2, \ldots, p, \quad i = 1, 2, \ldots, s \tag{61}$$

and $D(r) : \sum_{i=1}^{s} b_i c_i^{k-1} a_{ij} = k^{-1} b_j (1 - c_j^k), \quad k = 1, 2, \ldots, r, \quad j = 1, 2, \ldots, s$. (60) allows to write $\int_x^{x+h} \mathbf{F}(s)\mathrm{d}s \approx h\sum_{i=1}^{s} b_i \mathbf{F}(x + c_i h)$ which is exact for all polynomials with a degree lower than p. Moreover, if (60) is satisfied, the RK procedure has quadrature of order q.

Remark 12 If on the one hand the implicit RK methods require a greater implementation effort than the usual explicit procedures, on the other hand, they are well suited to be applied to non-linear differential problems such as the one under study (Quarteroni et al. 2007).

7.3.3 The three-stage Lobatto IIIa formula

Here, c_i must be chosen as roots of $P_s^* - P_{s-2}^* = \frac{d^{s-2}}{dx^{s-2}}(x^{s-1}(x-1)^{s-1})$, where s is the number of the stage, achieving $c_1 = 0$ and $c_s = 1$, $\forall s$ (Quarteroni et al. 2007). Let us introduce the two following definition useful for our purposes.

Definition 2 Let us consider the following mesh-grid

$$0 = a = r_0 < r_1 < \cdots < r_n = b = R \tag{62}$$

such that, on it, we define the step-size $h_m = r_{m+1} - r_m$.

Definition 3 Considering each range (r_m, r_{m-1}), we denote their midpoints by $r_{m+1/2}$ and, by $u_{m+1/2}$, the approximation of $u(r)$ at $r_{m+1/2}$.

Remark 13 $\mathbf{p}(r)$ (cubic polynomial) satisfy the boundary conditions as shown in (55) and moreover, $\forall(r_m, r_{m+1})$, (62) is considered. $\mathbf{p}(r)$ is located at the edges of each sub-interval and midpoint as well where $\mathbf{p}(r)$ is continuous.

This procedure is a collocation one and it is equivalent to the three-stage Lobatto IIIa implicit RK procedure (Quarteroni et al. 2007). Finally, it is derivable from (56) using the Simpson quadrature to approximate the integral between x_n and x.

Remark 14 $\mathbf{p}(r)$, with their derivatives, satisfy $\forall r \in (a, b)$, $\mathbf{p}^{(l)}(r) = \mathbf{u}^{(l)}(r) + \mathcal{O}(h^{4-l})$, $l = 0, 1, 2, 3$. Moreover, $\mathbf{p}(r)$ satisfies (55) at each intermediate point and at the midpoint of each interval. Furthermore, $\mathbf{p}(r)$ is selected by MatLab® determining some unknown parameters. Finally, it makes sense to write the following:

$$\mathbf{p}'(r_m) = \mathbf{F}[r_m, \mathbf{p}(r_m)]; \quad \mathbf{p}'(r_{m+1/2}) \tag{63}$$

$$= \mathbf{F}[r_{m+1/2}, \mathbf{p}(r_{m+1/2})], \quad \mathbf{p}'(r_{m+1}) = \mathbf{F}[r_{m+1}, \mathbf{p}(r_{m+1})] \tag{64}$$

which represents the non-linear equations solvable, for example, by a MatLab® solver. Furthermore, MatLab®, $\forall r \in (a, b)$, computes the cubic polynomial exploiting an its special routine (*bvpval*).

Remark 15 A BVP could have more than one solution. Therefore, it is imperative to have a guess for both the initial mesh and if possible, the solution. Thus, the MatLab® solver adapts the mesh achieving a solution by a selected number of mesh point.

Usually, giving a good initial hypothesis can be complicated. MatLab® solver checks a residue $\mathbf{res}(r) = \mathbf{p}'(r) - \mathbf{F}[r, \mathbf{p}(r)]$, while the boundary conditions becomes $\mathbf{g}[\mathbf{p}(a), \mathbf{p}(b)]$. Obviously, if $\mathbf{res}(r)$ is small, $\mathbf{p}(r)$ can be a good solution and if the problem is well-conditioned, $\mathbf{p}(r)$ is next to $\mathbf{u}(r)$. This is important because it helps us to recover the membrane profile with sufficient approximation. In this work, we have exploited MatLab® R2017a *bvp4c* solver because it implements the collocation procedure through a piece-wise cubic $\mathbf{p}(r)$ where its coefficients are determined in an order such that $\mathbf{p}(r)$ is continuous on (a, b). This continuity ensures that the membrane during deformation does not undergo tears or in any case abrupt local variations of its profile. Furthermore, the computation of both mesh and estimation error whose management is exploited to manage inadequate guesses for the mesh and the solution as well are based on the residual of $\mathbf{p}(r)$. Finally, this ToolBox performs a very reduced computational burden to obtain the Jacobian.

7.3.4 Four-stage Lobatto IIIa formula

This formula can be easily derived as an implicit RK method (Quarteroni et al. 2007). As the previous three-stage formula, this procedure can be considered a polynomial collocation whose solutions belong to $C^1([a, b])$ [1], showing a fifth-order accuracy. In this case, MatLab® solves this formula by finite different method, exploiting its *bvp5c* routine and solving the algebraic equation directly.

8 Some numerical tests

8.1 Some results of convergence

As shown in Versaci et al. (2020b), $\theta\lambda^2$ ensuring the convergence of all exploited procedure, indicated by $\min(\theta\lambda^2)_{\text{conv}}$ was obtained in the absence of a fringing field: if

[1] Again, this continuity protects us from dangerous tears in the membrane profile.

Table 1 Ranges of $\theta\lambda^2$ ensuring convergence (shooting and Keller-Box procedures)

δ	Shooting (ode 23)	Shooting (ode 45)	Keller-Box
0	$(\theta\lambda^2)_{\text{conv}} \in [0.630 \ +\infty)$	$(\theta\lambda^2)_{\text{conv}} \in [0.609 \ +\infty)$	$(\theta\lambda^2)_{\text{conv}} \in [0.619 \ +\infty)$
0.25	$(\theta\lambda^2)_{\text{conv}} \in [0.542 \ +\infty)$	$(\theta\lambda^2)_{\text{conv}} \in [0.540 \ +\infty)$	$(\theta\lambda^2)_{\text{conv}} \in [0.541 \ +\infty)$
0.5	$(\theta\lambda^2)_{\text{conv}} \in [0.483 \ +\infty)$	$(\theta\lambda^2)_{\text{conv}} \in [0.481 \ +\infty)$	$(\theta\lambda^2)_{\text{conv}} \in [0.582 \ +\infty)$
0.75	$(\theta\lambda^2)_{\text{conv}} \in [0.437 \ +\infty)$	$(\theta\lambda^2)_{\text{conv}} \in [0.434 \ +\infty)$	$(\theta\lambda^2)_{\text{conv}} \in [0.436 \ +\infty)$
1	$(\theta\lambda^2)_{\text{conv}} \in [0.398 \ +\infty)$	$(\theta\lambda^2)_{\text{conv}} \in [0.393 \ +\infty)$	$(\theta\lambda^2)_{\text{conv}} \in [0.395 \ +\infty)$
1.25	$(\theta\lambda^2)_{\text{conv}} \in [0.366 \ +\infty)$	$(\theta\lambda^2)_{\text{conv}} \in [0.361 \ +\infty)$	$(\theta\lambda^2)_{\text{conv}} \in [0.364 \ +\infty)$
1.5	$(\theta\lambda^2)_{\text{conv}} \in [0.338 \ +\infty)$	$(\theta\lambda^2)_{\text{conv}} \in [0.331 \ +\infty)$	$(\theta\lambda^2)_{\text{conv}} \in [0.332 \ +\infty)$
1.75	$(\theta\lambda^2)_{\text{conv}} \in [0.315 \ +\infty)$	$(\theta\lambda^2)_{\text{conv}} \in [0.307 \ +\infty)$	$(\theta\lambda^2)_{\text{conv}} \in [0.309 \ +\infty)$
1.99	$(\theta\lambda^2)_{\text{conv}} \in [0.294 \ +\infty)$	$(\theta\lambda^2)_{\text{conv}} \in [0.285 \ +\infty)$	$(\theta\lambda^2)_{\text{conv}} \in [0.287 \ +\infty)$

$\theta\lambda^2 < \min(\theta\lambda^2)_{\text{conv}}$ there was no convergence of all the numerical procedures; when $\theta\lambda^2 >\in (\theta\lambda^2)_{\text{conv}}$, all numerical procedures converged (in some cases, ghost solutions occurred). In this work, starting from (6), we obtained $(\theta\lambda^2)_{\text{conv}}$ exploiting shooting by ode23 and ode 45, Keller-Box scheme, III/IV Stage Lobatto IIIa formulas when $\delta \in [0, 2)$ increased, according to (19), to simulate the presence of the fringing field. Tables 1 and 2 shows that as δ increases and regardless of the numerical procedure used, the minimum value of $\theta\lambda^2$ that ensures convergence becomes smaller and smaller. This peculiarity is more evident in Fig. 2. In fact, as δ increases, a significant decrease in the minimum value of $\theta\lambda^2$ is observed. Furthermore, for values of δ close to 2, the convergence of the numerical procedures is ensured with values of $\theta\lambda^2$ that begin to diverge from each other (albeit in an extremely limited manner). Additionally, as δ increased, the profiles of the membrane were recovered using the above numerical procedures. As is evident from Fig. 3 and 4, as δ increases, the convergence of the numerical procedures is ensured by decreasing $\theta\lambda^2$. We also observe from Figs. 3 and 4 that although δ increases (in (6) δ appears in the denominator) and $\theta\lambda^2$ decreases (in (6) $\theta\lambda^2$ appears at denominator), the effect due to δ prevails over the effect due to $\theta\lambda^2$. This is because the profiles of the membrane flatten more and more as the intensity of the fringing field increases as with the intensification of the fringing field phenomenon (i.e., with the increase of δ), the direction lines of $\mathbf{E}$ deform significantly, hindering the deformation of the membrane toward the upper plate.

Remark 16 From Figs. 3 and 4, the membrane MEMS device studied in this work is not in the regime of large displacements because $\theta\lambda^2$ allow to obtain values of $u''(x)$ (see (3)) such as to have reduced concavity of the membrane profiles, making this device appropriate for biomedical applications such as intravenous drug delivery where small membrane shifts are required.

Remark 17 The membrane profiles numerically recovered are symmetric with respect to the vertical axis $x = 0$, highlighting that $\max\{|u'(x)|\}$ corresponds to $x = \pm L$ (Figs. 3, 4). Furthermore, $\max\{|u'(x)|\} < \sup\{|u'(x)|\} = H = 146$ Di Barba et al. (2021). Then, on $x = \pm L$, there is no risk of dangerous adhesion between the membrane and the vertical walls of the device which could generate unwanted electrostatic effects (phenomenon that occur if $|u'(\pm L)| \to +\infty$).

Table 2 Ranges of $\theta\lambda^2$ ensuring convergence (Three/Four Stage Lobatto IIIa)

δ	Three-Stage Lobatto IIIa (bpv4c)	Four-Stage Lobatto IIIa (bpv5c)
0	$(\theta\lambda^2)_{\text{conv}} \in [0.614\ +\infty)$	$(\theta\lambda^2)_{\text{conv}} \in [0.613\ +\infty)$
0.25	$(\theta\lambda^2)_{\text{conv}} \in [0.542\ +\infty)$	$(\theta\lambda^2)_{\text{conv}} \in [0.542\ +\infty)$
0.50	$(\theta\lambda^2)_{\text{conv}} \in [0.486\ +\infty)$	$(\theta\lambda^2)_{\text{conv}} \in [0.483\ +\infty)$
0.75	$(\theta\lambda^2)_{\text{conv}} \in [0.438\ +\infty)$	$(\theta\lambda^2)_{\text{conv}} \in [0.437\ +\infty)$
1	$(\theta\lambda^2)_{\text{conv}} \in [0.398\ +\infty)$	$(\theta\lambda^2)_{\text{conv}} \in [0.399\ +\infty)$
1.25	$(\theta\lambda^2)_{\text{conv}} \in [0.367\ +\infty)$	$(\theta\lambda^2)_{\text{conv}} \in [0.366\ +\infty)$
1.50	$(\theta\lambda^2)_{\text{conv}} \in [0.339\ +\infty)$	$(\theta\lambda^2)_{\text{conv}} \in [0.338\ +\infty)$
1.75	$(\theta\lambda^2)_{\text{conv}} \in [0.315\ +\infty)$	$(\theta\lambda^2)_{\text{conv}} \in [0.315\ +\infty)$
1.99	$(\theta\lambda^2)_{\text{conv}} \in [0.295\ +\infty)$	$(\theta\lambda^2)_{\text{conv}} \in [0.294\ +\infty)$

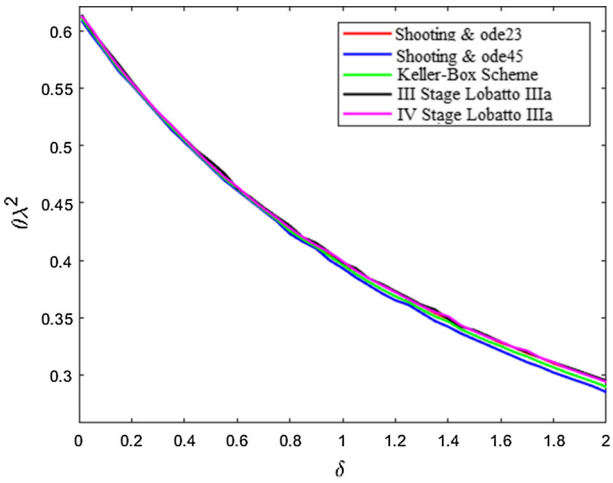

Fig. 2 Trend of $\theta\lambda^2$ as δ increases: the more intense the effect of the fringing field, the less $\theta\lambda^2$

8.2 Evaluation of eventuality of possible ghost solutions

As known, each numerical solution that does not satisfy the condition (20) represents a ghost solution. Therefore, from (20), we can write the following:

$$1 + H^6 < \frac{\theta\lambda^2}{24L(L+1)(1-\delta H^2)} = \frac{\theta\lambda^2}{18}\frac{1-\delta H^2+\delta H^2}{(1-\delta H^2)}$$
$$= \frac{\theta\lambda^2}{18}\left(1+\frac{\delta H^2}{(1-\delta H^2)}\right) \leq \frac{\theta\lambda^2}{18}(1+\delta H^2). \tag{65}$$

Then, considering (7), (65) becomes

$$1 + H^6 < \frac{\theta}{36}\frac{(1+\delta H^2)\epsilon_0 V^2}{d^3 T}, \tag{66}$$

[redacted]

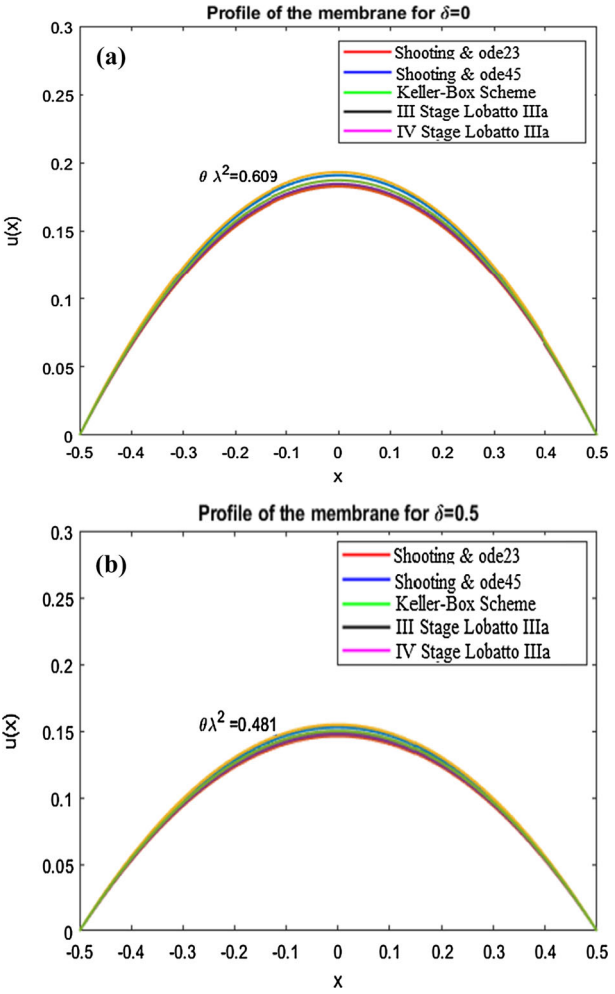

Fig. 3 $u(x)$ when shooting procedure and $ode23/ode45$, Keller-Box scheme, II/IV Stage Lobatto IIIa formulas have been applied: **a** $\theta\lambda^2 = 0.630$ with $\delta = 0$ and **b**)$\theta\lambda^2 = 0.582$ with $\delta = 0.5$

from which, being $\epsilon_0 = 8.85 \cdot 10^{-12}, \theta \approx 10^{14}, d = 10^{-9}, T = 10^{-4}$ (Pelesko and Bernstein 2003) and $H = 146$, we obtain the following:

$$V > \underbrace{\sqrt{\frac{36(1+H^6)d^3T}{\theta\epsilon_0(1+\delta H^2)}}}_{\inf\{V\}} = \frac{0.3905}{\sqrt{1+21316\delta}}. \tag{67}$$

Thus, analyzing the (67), without fringing field, to move the membrane $V > 0.3905$ Volts. The stronger the fringing effect, the lower the V needed to move the membrane. This is due to the fact that the lines of force of $\mathbf{E}$ near the edges of the device are curved towards the outside of the device itself, facilitating the deformation of the membrane; therefore, to move the membrane itself a smaller external V is required. Then, the greater the initial deformation of the lines of force of $\mathbf{E}$ (i.e., the greater the effect due to the fringing field) the lower the

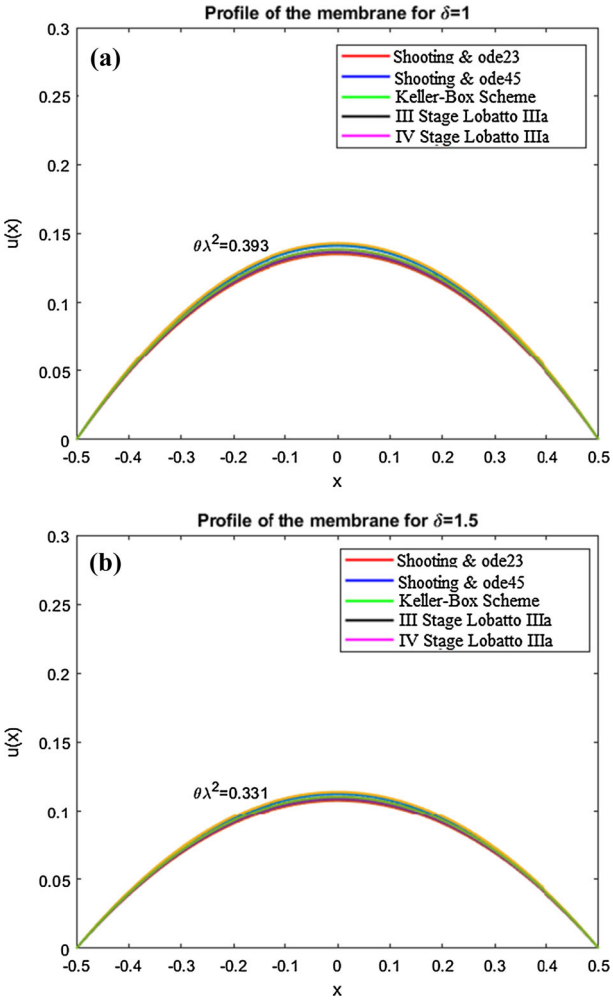

Fig. 4 $u(x)$ when shooting procedure and $ode23/ode45$, Keller-Box scheme, II/IV Stage Lobatto IIIa formulas have been applied: (a) $\theta\lambda^2 = 0.399$ with $\delta = 1$ and (b) $\theta\lambda^2 = 0.339$ with $\delta = 1.5$

tension V to move the membrane. This eventuality is of fundamental importance especially in cases where the membrane MEMS device is inserted in an electrical equipment for industrial or biomedical applications subjected to low electrical operating voltage (for example, micropumps for drug delivery systems). In these cases, the fringing field phenomenon helps to move the membrane easily, overcoming its mechanical inertia.

Remark 18 Under convergence conditions, $\forall\delta \in [0, 2)$, each numerical procedure produces a corresponding membrane profile. Let $u_j^\delta(x)$ be the membrane profile obtained by applying the j-th numerical procedure with a specific value of δ. Since $H = \sup|u'(x)|$, it follows that $H_j^\delta = \sup|u_j^\delta(x)|$. Since $H_j^\delta < H$, it is appropriate to write $1 + (H_j^\delta)^6 < 1 + H^6$, and considering the condition (65), we can write $1 + (H_j^\delta)_j < \frac{\theta\lambda^2}{18}(1 + \delta H^2)$, from which

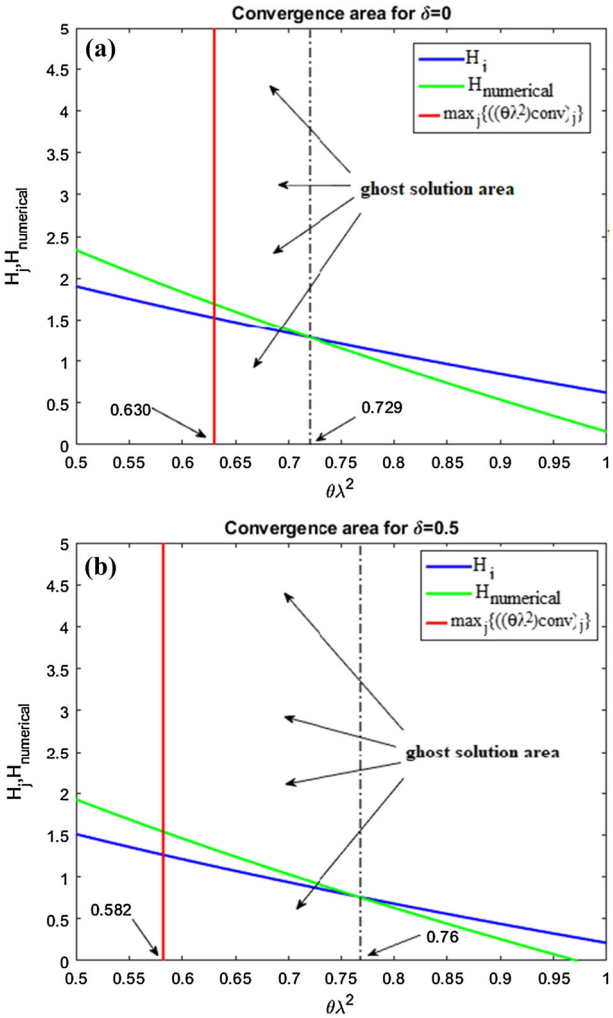

Fig. 5 H_j and $H_{\text{numerical}}$ depending on $\theta\lambda^2$ when $\delta = 0$ and $\delta = 0.5$, respectively

$$(H_j^{\delta}) < \sqrt[6]{\frac{\theta\lambda^2}{18}(1 + \delta H^2) - 1}. \tag{68}$$

The performances of (68) are shown in Figs. 5 and 6. Particularly, as δ increases, the trends of $\sup\{H_j^{\delta}\}$ and H (obtained numerically) are displayed, highlighting (using indicative arrows) the convergence areas of the numerical procedures with ghost solutions. We, finally, observe that (68), when $\delta = 0$ is the same inequality for H_j achieved in Versaci et al. (2019).

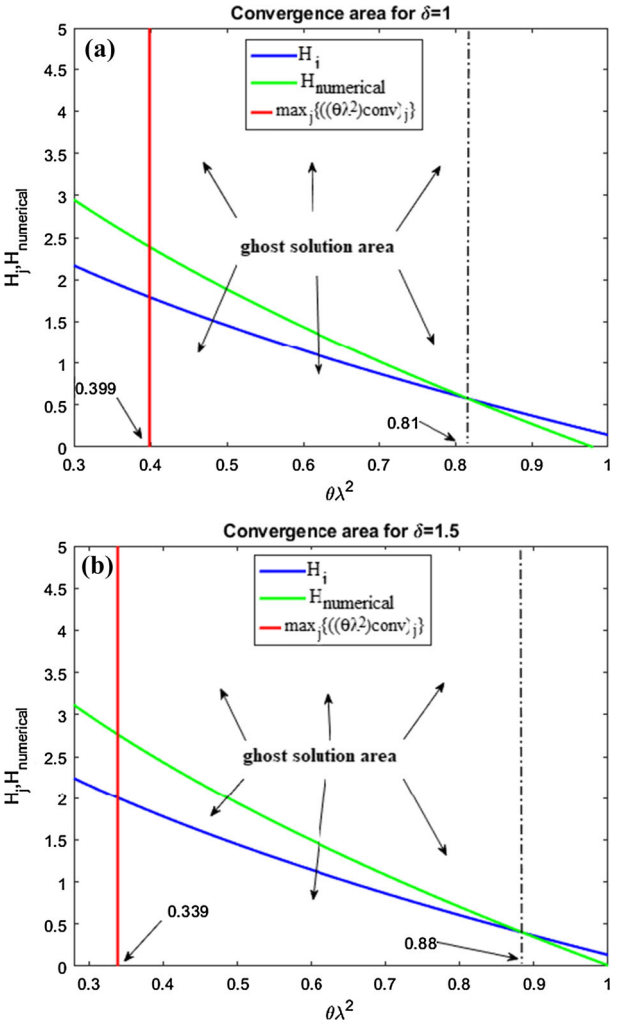

Fig. 6 H_j and $H_{\text{numerical}}$ depending on $\theta\lambda^2$ when $\delta = 1$ and $\delta = 1.5$, respectively

8.3 Electromechanical properties of the material constituting the membrane and operational parameters are not allowed in convergence areas

Multiplying both sides of (9) by λ^2 and again considering (7), we obtain the following:

$$\theta|\mathbf{E}|^2\lambda^2 = \frac{8\epsilon_0 L^4 V^4}{d^6 T^2 (1-u(x))^2}. \tag{69}$$

Moreover, being $|\mathbf{E}|^2 < \sup\{|\mathbf{E}|^2\}$, it follows $\frac{1}{|\mathbf{E}|^2} > \frac{1}{\sup\{|\mathbf{E}|^2\}}$ and, since $1-u(x) < 1$, it follows $\frac{1}{1-u(x)} > 1$. Thus, from (69), we achieve the following:

$$\theta\lambda^2 = \frac{8\epsilon_0 L^4 V^4}{d^6 T^2 (1-u(x))^2 |\mathbf{E}|^2} > \frac{8\epsilon_0 L^4 V^4}{d^6 T^2 \sup\{|\mathbf{E}|^2\}}. \tag{70}$$

[redacted]

Under non-convergence conditions of each numerical procedure used, it follows that

$$\theta\lambda^2 < \min_{j,\delta}\{((\theta\lambda^2)_{\text{conv}})_j^{\delta}\}, \tag{71}$$

so that (70) becomes

$$\min_{j,\delta}\{((\theta\lambda^2)_{\text{conv}})_j^{\delta}\} > \theta\lambda^2 > \frac{8\epsilon_0 L^4 V^4}{d^6 T^2 \sup\{|\mathbf{E}|^2\}}, \tag{72}$$

from which

$$T > \sqrt{\frac{8\epsilon_0 L^4 V^4}{d^6 \sup\{|\mathbf{E}|^2\} \min_{j,\delta}\{((\theta\lambda^2)_{\text{conv}})_j^{\delta}\}}}. \tag{73}$$

Therefore, once the intended use of the device has been fixed (i.e. fixed V which satisfies (67) and, consequently, also $\sup\{|\mathbf{E}|^2\}$ is fixed inside the device for a specific industrial or biomedical application), in conditions of non-convergence, all materials whose T satisfies (73) must be avoided. Conversely, if the membrane constituent material has been selected a priori (i.e. a particular value of T has been selected), in conditions of non-convergence, the intended uses of the device that satisfy

$$\frac{V^4}{\sup\{|\mathbf{E}|^2\}} < \frac{\min_{j,\delta}\{((\theta\lambda^2)_{\text{conv}})_j^{\delta}\} d^6 T^2}{8\epsilon_0 L^4} \tag{74}$$

are not allowed. Finally, we observe that in (74) the presence of fringing field effects are incorporated into $\min_{j,\delta}\{((\theta\lambda^2)_{\text{conv}})_j^{\delta}$. In other words, the concavity of the membrane profile, together with the geometric parameters of the device and the mechanical tension of the membrane, contribute to determining the operating electrostatic parameters of use of the device.

8.4 Electromechanical characteristics of the membrane material and operational parameters relating to any ghost solutions

In this case, if $\min_{j,\delta}\{((\theta\lambda^2)_{\text{conv}})_j^{\delta}\}_{\text{limit}}$ represents the value of $\theta\lambda^2$, in convergence conditions, below which we have ghost solutions, (69), in presence of ghost solutions, it satisfies the following condition:

$$\min_{j,\delta}\{((\theta\lambda^2)_{\text{conv}})_j^{\delta}\} < \frac{8\epsilon_0 L^4 V^4}{d^6 T^2 \sup\{|\mathbf{E}|^2\}} < \min_{j,\delta}\{((\theta\lambda^2)_{\text{conv}})_j^{\delta}\}_{\text{limit}} \tag{75}$$

from which

$$\frac{d^6 T^2 \min_{j,\delta}\{((\theta\lambda^2)_{\text{conv}})_j^{\delta}\}}{8\epsilon_0 L^4} < \frac{V^4}{\sup\{|\mathbf{E}|^2\}} < \frac{d^6 T^2 \min_{j,\delta}\{((\theta\lambda^2)_{\text{conv}})_j^{\delta}\}_{\text{limit}}}{8\epsilon_0 L^4}. \tag{76}$$

Then, having chosen the intended use of the device, i.e., having fixed V satisfactorily, the (67) and therefore also $\sup\{|\mathbf{E}|^2\}$ (in other words, having fixed a particular industrial or biomedical application), T of the material constituting the membrane must satisfy the (76). Conversely, from (75), we can write the following:

$$\frac{d^6 \min_{j,\delta}\{((\theta\lambda^2)_{\text{conv}})_j^{\delta}\} \sup\{|\mathbf{E}|^2\}}{8\epsilon_0 L^4 V^4} < \frac{1}{T^2} < \frac{d^6 \min_{j,\delta}\{((\theta\lambda^2)_{\text{conv}})_j^{\delta}\}_{\text{limit}} \sup |\mathbf{E}|^2}{8\epsilon_0 L^4 V^4}. \tag{77}$$

[redacted]

Then, once the membrane material has been chosen (that is, once T, V has been selected, in addition to satisfying the condition (67), together with $\sup\{|\mathbf{E}|^2\}$, it must also satisfy the condition (77).

Remark 19 It is noteworthy that the range of $\theta\lambda^2$ characterized by the presence of ghost solutions represents, electrostatically, a problem because the profiles achieved numerically, in fact, do not satisfy the analytical model. Thus, this range is required to be as small as possible. Therefore, from (76) we can easily write the following:

$$(\min_{j,\delta}\{((\theta\lambda^2)_{\text{conv}})_j^{\delta}\} - \min_{j,\delta}\{((\theta\lambda^2)_{\text{conv}})_j^{\delta}\}_{\text{limit}}) < \frac{V^4}{\sup\{|\mathbf{E}|^2\}}\frac{1}{T^2}\frac{8\epsilon_0 L^4}{d^6}. \tag{78}$$

Particularly, (78) shows promising potential. In fact, once the geometry of the device is fixed (ie, fixed L and d), the higher the membrane voltage T, the lower the range of values of $\theta\lambda^2$ at risk of having ghost solutions. Therefore, rigid membranes do not allow large margins for the presence of ghost solutions. Moreover, the higher the $\frac{V^4}{\sup\{|\mathbf{E}|^2\}}$ ratio, the greater the area dedicated to ghost solutions. In other words, once the geometry of the device is fixed, the intended uses that require high values of V have higher risks of obtaining ghost solutions. In these cases, the device can be used in all those applications where reduced voltage values ãâare required to avoid the presence of ghost solutions.

8.5 Electromechanical characteristics of the membrane material and operating parameters in conditions of convergence and in the absence of ghost solutions

Finally, if V ([2]), $\sup\{|\mathbf{E}|\}$ and T satisfy

$$\frac{8\epsilon_0 L^4 V^4}{d^6 T^2 \sup\{|\mathbf{E}|^2\}} > \min_{j,\delta}\{((\theta\lambda^2)_{\text{conv}})_j^{\delta}\}_{\text{limit}} \tag{79}$$

we are working in conditions of convergence without ghost solutions. So, given the values of V and $\sup\{|\mathbf{E}|^2\}$ (once V satisfies (67)), T must satisfy the following condition:

$$\frac{1}{T^2} > \frac{d^6 \min_{j,\delta}\{((\theta\lambda^2)_{\text{conv}})_j^{\delta}\}_{\text{limit}} \sup\{|\mathbf{E}|^2\}}{8\epsilon_0 L^4 V^4}. \tag{80}$$

Vice-versa, once T is fixed, V and $\sup\{|\mathbf{E}|^2\}$ must satisfy (80).

Remark 20 (79) is a limitation on the range of $\theta\lambda^2$ intended for ghost solutions. Particularly, once the geometry of the device is fixed (i.e., once L and d are fixed) membranes characterized by high mechanical tensions T limit the presence of ghost solutions. On the other hand, intended uses of the device that require high values of V increase the risks of ghost solutions. Therefore, in these cases, MEMS devices with high stiffness membranes destined for applications are to be preferred if the electrical operating voltages are reduced.

9 Conclusions and perspectives

In this paper, the profile of the membrane, $u(x)$, in a membrane MEMS device in dimensionless $1D$ geometry was recovered when an external electrical voltage V was applied. Inside

[2] Obviously, V must also satisfy (67).

the device, once V is applied, the membrane deforms toward the plate subjected to a higher potential. Moreover, V, inside the device generates $\mathbf{E}$ locally orthogonal to the tangent line to the membrane at the same point. Considering that the greater $|\mathbf{E}|$, the more the membrane bends, it was assumed that $|\mathbf{E}|$ is locally proportional to the curvature $K(x, u(x))$ of the membrane. Furthermore, to consider the fringing field phenomenon, an addend was incorporated in the model, weighted by a parameter δ which was found to belong to the interval $[0, 2)$, depending on $|u'(x)|^2$. This considers the deformation of the $\mathbf{E}$ lines of force near the edges of the device. For the already known algebraic condition ensuring the existence of the solution for the problem under study, in this paper, an algebraic condition was obtained from a new algebraic condition ensuring the uniqueness of the solution depending on the electromechanical properties of the membrane material which, after careful analysis, was stronger than the condition of existence. The profile of the membrane was recovered using different numerical procedures (shooting, Keller-Box, III/IV stage Lobatto IIIA formulas) whose performances were compared with each other, also obtaining, the respective intervals of $\theta\lambda^2$ (which manages the amplitude of the concavity of the deformed membrane) and ensuring the convergence. Finally, the link between the electromechanical properties of the membrane material and the operating parameters were obtained both in conditions of non-convergence and convergence with and without ghost solutions. From the analysis of the results, it is evident that the performances of the numerical procedures used are equivalent. This is because any δ and for each range of $\theta\lambda^2$ ensuring convergence, the discrepancy in behavior is negligible. It is noteworthy that as the effect due to the fringing field increases (increase of δ), the areas in the $\theta\lambda^2 - H$ plane characterized by the presence of ghost solutions becomes more extensive but nevertheless limited. IT thus allows contained real displacements of the membrane (low values of H) that can still modify the electrostatic capacity of the device with respect to the condition in which the membrane is at rest. This makes the device studied attractive for many biomedical applications such as, for example, devices for the diffusion of drugs via intravenous in which sudden deformations of the membrane of a small entity are required. Finally, the link between the electromechanical properties of the membrane material and the operating parameters does not depend on δ. In other words, this bond is independent of the deformation of the $\mathbf{E}$ lines of force near the edges of the device. This makes it possible to use this link as a valid tool which, starting from the type of device, determines its intended use and vice versa.

References

Ali IA (2012) Modeling and simulation of MEMS components: challenges and possible solutions. Micromachining techniques for fabrication o micro and nano structures. Springer Nature, Singapore

Angiulli G, Jannelli A, Morabito FC, Versaci M (2018) Recondtruting the membrane detection of a $1D$ electrostatic-driven MEMS device by the shooting method: convergence analysis and ghost solutions identification. Comput Appl Math 37:4484–4498. https://doi.org/10.1007/s40314-017-0564-4

Batra RC, Porfiri M, Spinello D (2006) Electromechanical model of electrically actuated narrow microbeams. J Microelectromech Syst 15(5):1175–1189

Batra RC, Porfiri M, Spinello D (2006) Micro Nano Lett 1:2

Batra RC, Porfiri M, Spinello D (2007) Review of modeling electrostatically actuated microelectromechanical systems. Smart Mater Struct 16:6

Bayley PB, Shampine LF, Waltman PE (1969) Nonlinear two points boundary value problems. Academic Press, New York

Bechtold T, Schrag G, Feng L (2013) System-level modeling of MEMS. Wiley, London

Cassani D, Tarsia A (2016) Periodic solutions to nonlocal MEMS equations. Discret Contin Dyn Syst Ser S 9(3):631–642

Cassani D, d'O M, Ghoussoub N (2009) On a fourth order elliptic problem with a singular nonlinearity. Nonlinear Stud 9:189–209
Cassani D, Fattorusso L, Tarsia A (2014) Nonlocal dynamic problems with singular nonlinearities and application to MEMS. Nonlinear Differ Equ Appl 85:185–206
Cassani D, Fattorusso L, Tarsia A (2013) Nonlocal singular problems and application to MEMS. In: Proceedings of world congress on engineering, pp 155–164
Cauchi M et al (2018) Analytical, numerical and experimental study of a horizontal electrothermal MEMS microgripper of the deformability charcterization of human red blood cells. Micromachines 9(3):108–119
Chen YX et al (2019) Fringing field effect analysis of parallel plate capacitors for capacitive power transfer application. In: Proceedings of 4th IEEE international future energy electronics conference, pp 115–120
de Oliveira Hansen R et al (2018) Magnetic films for electromagnetic actuation ibn MEMS switches. Microsyst Technol 24:10
Di Barba P, Wiak S (2020) MEMS: field models and optimal design. Springer, Berlin
Di Barba P, Fattorusso L, Versaci M (2017) Electrostatic field in terms of geometric curvature in membrane MEMS devices. Commun Appl Ind Math 8(1):165–184
Di Barba P, Gotsalk T, Majastrzyk W, Mognaschi M, Orlowska K (2018) Optimal design of electromagnetically actuated MEMS cantilevers. Sensors 18(8):25–33
Di Barba P, Fattorusso L, Versaci M (2019) A 2*D* non-linear second-order differential model for electrostatic circular membrane MEMS devices: a result of existence and uniqueness. Mathematics 7(1193):1–18
Di Barba P, Fattorusso L, Versaci M (2020) Curvature dependent electrostatic field in the deformable MEMS device: stability and optimal control. Commun Appl Ind Math 11(1):35–54
Di Barba P, Fattorusso L, Versaci M (2021) Curvature-dependent electrostatic field as a principle for modelling membrane MEMS device with fringing field. Comput Appl Math 40(3):87
Farokhi H, Ghayesh MH (2017) Nonlinear thermo-mechanical behaviour of MEMS resonators. Microsyst Technol 23:5303–5315
Fento J, Liu C, Zhang W, Hao S (2018) Static and dynamic mechanical behaviors of electrostatic MEMS resonator with surface processing error. Micromach MDPI 9(34):1–29
Gad-el-Hak M (2006) MEMS: design and fabrication. Chapman & Hall, New York
Gallalgher E, Moussa W (2014) A study of the effect of the fringing fields on the electrostatic force in vertical comb drives. Sensors 1:20149–20164
Howell LL, Luon SM (2004) Thermomechanical in-plane microactuator (TIM), U.S. Patent N. 6
Javaheri H, Ghanati PP, Azizi S (2018) A case study on the numerical solution and reduced order model of MEMS. Sens MDPI 19:3
Leus V, Elata V (2004) Fringing field effect in electrostatic actuator. Technical Report ETR-2004-2
Mistry KK, Mahapatra A (2012) Design and simulation of a thermo-transfer type MEMS based micro flow sensor for arterial blood flow measurement. Microsyst Technol 18(6):683–692
Mohammad TF, Oukad HM (2016) Static, eigenvalue problem and bifurcation analysis of MEMS arches actuated by electrostatic fringing-fields. Microsyst Technol 22:193–206
Mohammadi A, Ali N (2015) Effect of high electrostatic actuation on thermoelastic damping in thin rectangular microplate resonators. J Theoret Appl Mech 53(2):317–3209
Nathanson H, Newell W, Wickstrom R, Lewis J (1964) The resonant gate transistor. IEEE Trans Electron Devices 14:117–133
Oukad HM (2014) Static response and natural frequencies of microbeams actuated by out-of-plane electrostatic fringing-fields. Int J Non-Linear Mech 62:39–48
Oukad HM (2018) Electrostatic fringing-fields effects on the structural behavior of MEMS shallow arches. Microsyst Technol 24:1391–1399
Pelesko JA, Bernstein DH (2003) Modeling MEMS and NEMS. CRC Press, Boca Raton
Pelesko JA, Driscoll TA (2005) The effect of the small-aspect-ratio approximation on canonical electrostatic MEMS models. J Eng Math 53:239–252
Quarteroni A, Sacco R, Saleri F (2007) Numerical mathematics. Springer, Berlin
Ren Z et al (2020) Thermo-mechanical modeling and experimental validation for multilayered metallic microstructures. Microsyst Technol 21:751–783
Velosa-Moncada L et al (2018) Design of a novel MEMS microgripper with rotatory electrostatic combdrive actuators for biomedical applications. Sensors 18(15):1–16
Versaci M, Morabito FC (2019) Membrane micro electro-mechanical systems for industrial applications, handbook of research on advanced mechatronic systems and intelligent. Robotics 20:139–175
Versaci M, Angiulli G, Fattoryusso L, Jannelli A (2019) On the uniqueness of the solution for a semi-linear elliptic boundary value problem of the membrane MEMS device for the recostructing the membrane profile in absence of ghost solutions. Int J Non-Linear Mech 109:24–31

Versaci M, Di Barba P, Morabito FC (2020) Curvature-dependent electrostatic field as a principle for modelling membrane-based MEMS devices. A review. Membr MDPI 10(11):1–51
Versaci M, Jannelli A, Angiulli G (2020) Electrostatic Micro-Electromechanical-Systems (MEMS) Devices: a Comparison Among Numerical techniques for recovering the membrane profile. IEEE Access 8:125874–125886
Vinyas M, Kattimani S (2018) Investigation of the Effect of $BaTiO_3 - CoFe_{24}$ Particle Arrangement on the Static Response of magneto-electro-thermo-elastic plates. Compos Struct 185:51–56
Wei J, Ye D (2010) On MEMS equation with fringing field. Proc Am Math Soc 138(2):1693–1699
Weng CC, Kong JA (1980) Effects of fringing fields on the capacitance of circular microstrip disk. IEEE Trans Microw Theory Tech 28(2):98–104
Yu Y et al (2012) Numerical and analytical approximations to large post-buckling deformation of MEMS. Int J Mech Sci 55(1):95–103
Zega V, Frang A, Guercilena A (2018) Analysis of frequency stability and thermoelastic effects for slotted tuning fork MEMS resonators. Sensors 8(7):1–15
Zhang Y et al (2018) Micro electrostatic energy harvester with both broad bandwidth and high normalized power density. Appl Energy 212:363–371
Zhao X et al (2004) A reduced-order model for electrically actuated microplates. J Micromech Microeng 14:7
Zozulya VV, Saez A (2016) A high-order theory of a thermoelastic beams and its application to the MEMS/NEMS analysis and simulations. Arch Appl Mech 86:1255–1273